ISTITUTO NAZIONALE DI RICERCA METROLOGICA
Repository Istituzionale

Measurement of the heat flux normalized spin Seebeck coefficient of thin films as a function of temperature

(Article begins on next page)

Measurement of the heat flux normalized spin Seebeck coefficient of thin films as a function of temperature

G. Venkat (iD), C. D. W. Cox (iD), A. Sola (iD), V. Basso (iD), and K. Morrison (iD)

View Online   Export Citation   CrossMark

ARTICLES YOU MAY BE INTERESTED IN
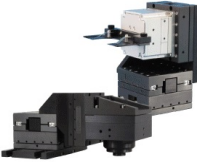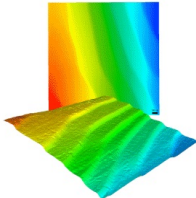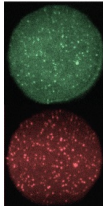
Nanopositioning Systems

Modular Motion Control

AFM and NSOM Instruments

Single Molecule Microscopes

MCL
MAD CITY LABS INC.
www.madcitylabs.com

Measurement of the heat flux normalized spin Seebeck coefficient of thin films as a function of temperature

G. Venkat,[1,a] (iD) C. D. W. Cox,[1] (iD) A. Sola,[2] (iD) V. Basso,[2] (iD) and K. Morrison[1,b] (iD)

AFFILIATIONS

[1] Department of Physics, Loughborough University, Loughborough LE11 3TU, United Kingdom
[2] Instituto Nazionale di Ricerca Metrologica, Strada delle Cacce 91, 10135 Torino, Italy

[a] Author to whom correspondence should be addressed: guruvenkat7@gmail.com. **Present address:** Department of Materials Science and Engineering, University of Sheffield, Sheffield S10 2TG, United Kingdom.
[b] **Email:** k.morrison@lboro.ac.uk

ABSTRACT

The spin Seebeck effect (SSE) has generated interest in the thermoelectric and magnetic communities for potential high efficiency energy harvesting applications and spintronic communities as a source of pure spin current. Understanding the underlying mechanisms requires characterization of potential materials across a range of temperatures; however, for thin films, the default measurement of an applied temperature gradient (across the sample) has been shown to be compromised by the presence of thermal resistances. Here, we demonstrate a method to perform low temperature SSE measurements where, instead of monitoring the temperature gradient, the heat flux passing through the sample is measured using two calibrated heat flux sensors. This has the advantage of measuring the heat loss through the sample as well as providing a reliable method to normalize the SSE response of thin film samples. We demonstrate this method with an $SiO_2/Fe_3O_4/Pt$ sample where a semiconducting–insulating transition occurs at the Verwey transition, T_V, of Fe_3O_4 and quantify the thermomagnetic response above and below T_V.

Published under license by AIP Publishing. https://doi.org/10.1063/5.0007989

I. INTRODUCTION

The spin Seebeck effect (SSE) was demonstrated in 2008 by Uchida *et al.*[1] and has since been widely studied from the perspective of improving the efficiency of thermoelectric devices for energy harvesting.[2] While it was initially demonstrated in the transverse configuration in a metallic system such as Pt/NiFe,[1] it was shortly thereafter measured in the longitudinal configuration in magnetic insulators such as Yttrium Iron Garnet (YIG), which removes parasitic effects such as the planar Nernst effect in the SSE response,[3] as well as being ideally suited for energy harvesting applications. The SSE has subsequently been measured in a variety of systems such as ferromagnetic semiconductors,[4] antiferromagnets,[5] paramagnets,[6] and ferrimagnets.[7]

In the longitudinal configuration, the SSE involves application of a temperature gradient (∇T) normal to the plane of a thin film with the magnetization (M) in the plane, which generates a spin

current (J_s) along the direction of ∇T. For detection, J_s is then converted to a transverse charge current in a material with high spin–orbit coupling via the inverse spin Hall effect (ISHE). Then, the voltage is measured,

$$V_{ISHE} = \frac{1}{2}\left(V_{sample}\big|_{M_{sat}^+} - V_{sample}\big|_{M_{sat}^-} \right), \qquad (1)$$

where M_{sat}^+ and M_{sat}^- are fields of positive and negative saturation and $V_{sample} = V_{ISHE} + V_S$ with V_S being the background voltage due to the ordinary Seebeck effect. In most studies, a heater is used to establish a temperature gradient across the sample. The temperature difference (ΔT) across the sample stack is usually measured with thermocouples in order to normalize V_{ISHE} as[8,9]

$$S_{\nabla T} = \left(\frac{V_{ISHE}}{L_y} \right) \cdot \left(\frac{L_z}{\Delta T} \right), \qquad (2)$$

where L_y is the contact separation and $\nabla T = \frac{\Delta T}{L_z}$, where L_z is the sample thickness. As it is the temperature gradient across the magnetic layer that drives the SSE, ΔT and L_z should describe the temperature difference and thickness of the magnetic layer itself (not including the substrate).[7] Unfortunately, in the literature, L_z has been defined interchangeably as the sample thickness (including substrate) or the thickness of the magnetic layer, which can complicate comparison of similar samples.[7]

However, it has been shown that $S_{\nabla T}$ is an unreliable measure of the SSE in thin films due to the presence of thermal interface resistances across the sample stack.[9] To circumvent this problem, Sola *et al.* defined a heat flux based coefficient,[10]

$$S_{J_Q} = \frac{V_{\text{ISHE}}}{J_Q L_y}, \tag{3}$$

where $J_Q = \frac{Q}{A}$ is the heat flux passing through the sample (Q is the heat applied and A is the cross-sectional area of the sample). S_{J_Q} has been shown to be a more reliable measure of the SSE, especially for thin films, and has been used to quantify the SSE performance of YIG:Pt,[8,9] Fe_3O_4:Pt,[11] $NiFe_2O_4$:Pd,[12] and Co_2MnSi:Pt.[13] This measurement has the advantage of being insensitive to thermal interface resistances in the measurement, as well as any thermal shunting across the thin film's substrate. Additionally, by multiplying Eq. (3) by the thermal conductivity of the magnetic film, the temperature normalized coefficient [defined in Eq. (2)] can be obtained.

In reports of low temperature SSE (LTSSE) measurements, either $S_{\nabla T}$ is quoted or S_{J_Q} is estimated assuming that the power, Q, supplied to the heater passes through the sample without loss.[14–16] This is not reliable as low temperature thermal measurements are susceptible to multiple sources of heat loss and is compounded by the fact that it is often difficult to find low temperature heat flux sensors (HFSs). This is also true of measurements where a lithographically patterned on-chip heater is used,[17,18] which, although allowing for measuring the signals from smaller samples, do not allow for the accurate determination of S_{J_Q}. Nevertheless, there is a need to measure S_{J_Q} down to low temperatures so that the interplay of different mechanisms (a metal-insulating transition may result in a shift from spin dependent- to magnon spin-Seebeck driven spin current)[2,11] or the impact of magnetic and structural phase transitions (on the signal) can be studied.[5,6] It is also important to quantify the performance of materials, which shows an increase in their SSE response at low temperatures.[19]

We describe here a low temperature SSE (LTSSE) measurement setup to measure S_{J_Q} between 50 K and 300 K using a closed cycle refrigerator (CCR) cryostat. The heat flux through the sample is measured with Peltier sensors on either side of the sample. Measuring Fe_3O_4 (80 nm):Pt (5 nm) thin films deposited on glass, we observe a decrease in S_{J_Q} with temperature which we attribute to a general decrease in magnon accumulation.

II. MEASUREMENT SETUP

Figure 1(a) shows a schematic of the measurement setup. An oxygen-free high thermal conductivity (OFHTC) copper mount was fabricated to attach to the cold head of an ARS CCR cryostat, where an indium seal was used between the cold head and the measurement puck to provide good thermal contact. The sample was held

between two heat flux sensors (HFSs), which, in turn, were attached to copper blocks. The design is based on a central pillar, which is held at T_{base}, around which the thermal circuit is created [Fig. 1(c)]. A thermal gradient can be established by two activating Peltier cells (P_1 and P_2) wired in series such that a hot side ($T_{\text{base}} + \Delta T$) is created on an adjoining copper strip and a cold side ($T_{\text{base}} - \Delta T$) on the second copper strip. The heat from the hot side then traverses the copper strip and through the copper block and sample stack, as shown in Fig. 1(c). As two HFSs are used (P_3 and P_4), one on either side of the sample, a direct determination of the heat flux is obtained, and knowledge of the power generated by the heat source is not required. While the activating Peltiers could provide enough heating power to establish a thermal circuit and detect an SSE signal at higher temperatures, two 0.5 kΩ resistors were also secured to the pillars to provide additional heating power if needed (also for calibration of the HFSs). The components and signal pins were secured to the copper holder using thermal epoxy (Stycast 1266) to ensure mechanical stability and good heat flow [Fig. 1(b)].

A. Calibration procedure

The calibration of the HFSs is important for precise determination of J_Q and follows the procedure outlined by Sola *et al.*[10] The calibration was done in two modes: (a) heating from the top side(s) of the two HFSs and (b) heating from between the two HFSs.

In mode (a), the resistors R_1 and R_2 (shown in Fig. 1) were first used (in turn) to heat the HFSs from outside the stack such that an unknown heat, Q, passed through P_3 and P_4. This measurement enables determination of the relative sensitivity of each HFSs (to the other), and any difference between these measurements when heating with R_1 or R_2 is assumed to be due to heat loss through the HFSs. Upon the application of a heating current, the HFSs were allowed to equilibrate and settle (transient measurement), as shown in Fig. 2(a). The value of the Peltier HFS voltage V_P once equilibrium was reached (typically ~10 min to 30 min) was determined for different heating currents supplied to R_1/R_2 and as a function of temperature. The ratio of the responses of P_3 and P_4 was then determined,

$$f = \frac{V_{P_4}}{V_{P_3}}, \tag{4}$$

and is shown in Fig. 2(b). Note that the ~5% difference of the ratio measured for R_1 and R_2 is due to minor asymmetry in the heat losses from the HFSs. As we approach 300 K, there is also some divergence likely due to melting of the Apiezon N$^{\text{TM}}$ thermal grease used as the thermal interface between P_3 and P_4. With regard to asymmetry of the heat loss, heating from R_1, the expected voltage response could be described as

$$V_{P_3} = Q_{\text{in}} S_{P_3}, \tag{5}$$

$$V_{P_4} = (Q_{\text{in}} - Q_{\text{loss}}) S_{P_4}, \tag{6}$$

whereas heating from R_2,

$$V'_{P_4} = Q_{\text{in}} S_{P_4}, \tag{7}$$

$$V'_{P_3} = (Q_{\text{in}} - Q_{\text{loss}}) S_{P_3}, \tag{8}$$

where V_{P_3} and V_{P_4} are the voltages measured from HFSs P_3 and P_4, respectively, S_{P_3} and S_{P_4} are the corresponding sensitivities (V/W), Q_{in} is the heat that passes into the HFS assembly, and Q_{loss} is the
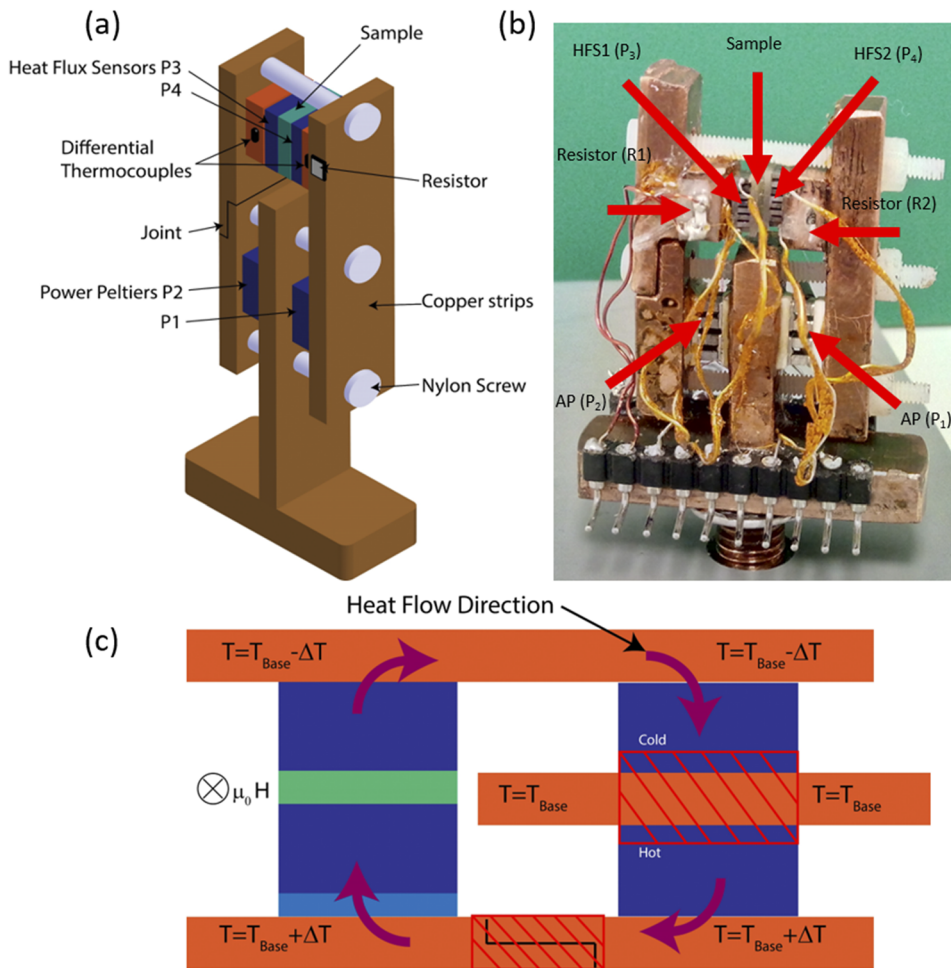
FIG. 1. The low temperature SSE (LTSSE) insert. (a) Schematic of the LTSSE holder showing the different components and (b) the corresponding photograph of the holder. (c) Schematic of the heat flow when setting up the temperature gradient using the activating Peltiers. The shaded areas indicate surfaces where thermal resistance of the circuit can be modified with the use of thermal grease, stycast, or indium as interface materials. In our measurements, we used Apiezon grease.

heat loss at each HFS. The difference in V_{P_4}/V_{P_3} when heating with R_1 and R_2 can therefore be attributed to the asymmetry of Q_{loss} with respect to Q_{in}, V_{P_3}, and V_{P_4}. Assuming that Q_{loss} is small with respect to Q_{in}, the average of V_{P_4}/V_{P_3} and V'_{P_4}/V'_{P_3} will give the ratio of S_{p4} to S_{p3} as follows:

$$\frac{V_{P_4}}{V_{P_3}} = \frac{(Q_{in} - Q_{loss})}{Q_{in}} \frac{S_{P_4}}{S_{P_3}}, \tag{9}$$

$$\frac{V'_{P_4}}{V'_{P_3}} = \frac{Q_{in}}{(Q_{in} - Q_{loss})} \frac{S_{P_4}}{S_{P_3}}, \tag{10}$$

$$\left(\frac{V_{P_4}}{V_{P_3}} + \frac{V'_{P_4}}{V'_{P_3}}\right) = \frac{(Q_{in} - Q_{loss})}{Q_{in}} \frac{S_{P_4}}{S_{P_3}} + \frac{Q_{in}}{(Q_{in} - Q_{loss})} \frac{S_{P_4}}{S_{P_3}}$$
$$= \frac{S_{P_4}}{S_{P_3}} \left(\frac{2Q_{in}^2 - 2Q_{in}Q_{loss} + Q_{loss}^2}{Q_{in}^2 - Q_{in}Q_{loss}}\right). \tag{11}$$

Where Q_{loss}^2 is considered negligible with respect to $2Q_{in}Q_{loss}$ and $2Q_{in}^2$, this reduces to

$$\frac{1}{2}\left(\frac{V_{P_4}}{V_{P_3}} + \frac{V'_{P_4}}{V'_{P_3}}\right) = \frac{S_{P_4}}{S_{P_3}}. \tag{12}$$

Therefore, the average of the calibration measurements in mode (a) will give the ratio of HFS sensitivities, S_{p4}/S_{p3}. For example, for the data shown in Fig. 2, V_{P_4}/V_{P_3} and V'_{P_4}/V'_{P_3} were 0.99 and 1.045, respectively. The average of this is 1.0175, which indicates that S_{P_4} = 1.0175 S_{P_3}. Inserting into Eqs. (9) or (10) indicates a Q_{loss} of 2.6% (of Q_{in}). For comparison, for Q_{in} = 1 W, this would give Q_{loss}^2 = 6.835 × 10^{-4} W^2 compared to $2Q_{in}^2$ = 2 W^2 and $2Q_{in}Q_{loss}$ = 0.052 W^2 [hence, the assumption made for Eq. (12) holds].

Mode (b) of the calibration requires heating of the HFSs by a resistor placed between them. In this scenario, Q is known and is assumed to pass through either P_3 or P_4 with negligible loss. To limit heat loss from the heater wires (conductive) or sides (radiative), a thin film strain gauge was used. A series of heating currents were supplied, while the voltage drop across the strain gauge was monitored (4 wire measurement) so that the total power (Q) supplied to the 2 HFSs could be determined. An example of the transient responses from each HFS at 50 K is shown in Fig. 2(c). Note that the response of P_3 is initially quite high and decreases as equilibrium is reached, while the response of P_4 increases. This demonstrates the different timescales associated with each HFS due to the joint
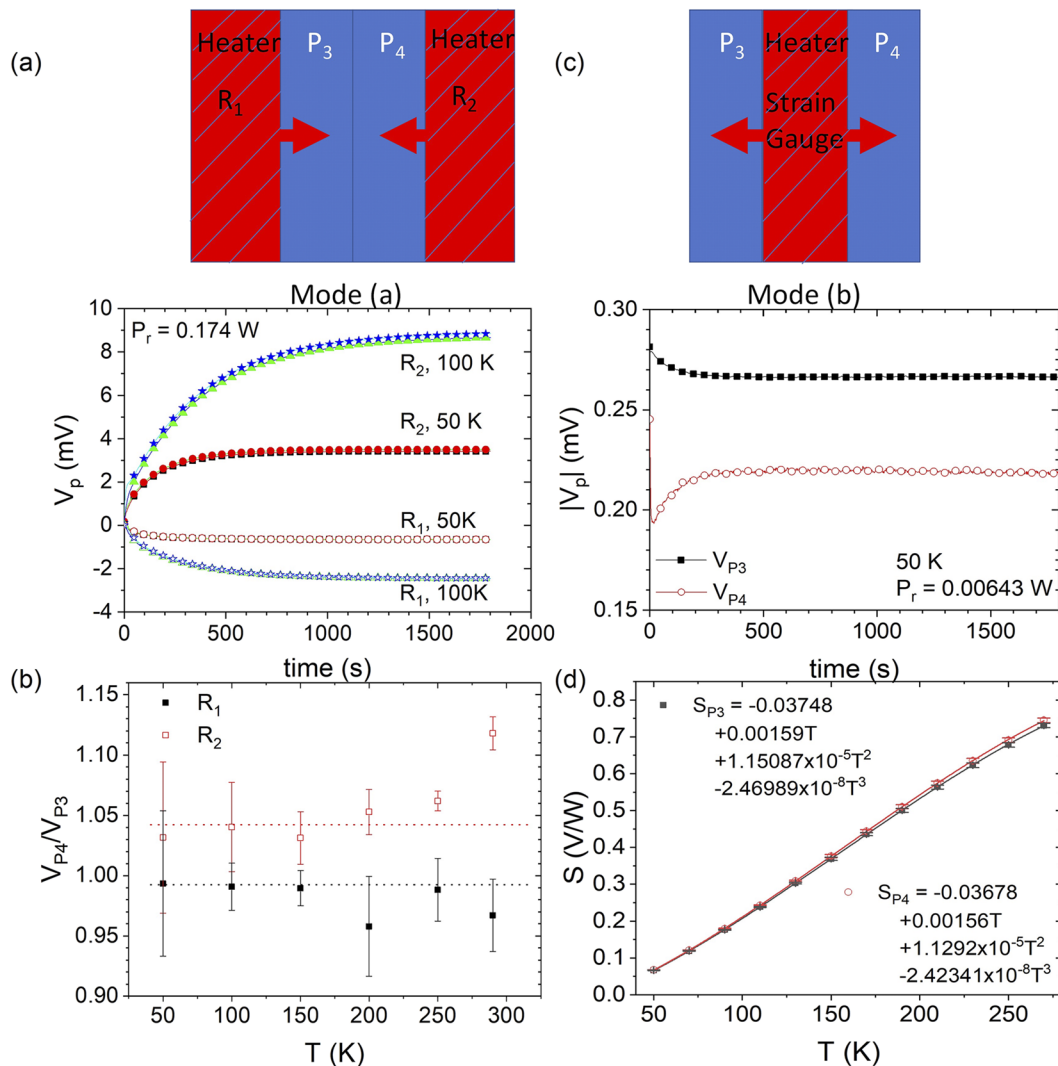
FIG. 2. Example data from Peltier calibrations. (a) The transient measurement signals from mode (a) where P_3 and P_4 are monitored while heated by R_1 (open symbols) or R_2 (closed symbols). (b) Corresponding ratio of V_{P_4}/V_{P_3} as a function of temperature. (c) Example transient measurements from mode (b) where the total heat, Q, is known but split between P_3 and P_4. (d) Summary of the calibration coefficients, S_3 and S_4, as a function of temperature (discussed in the text). (The upper schematics show the heater configurations and directions of heat flow in each calibration mode.)

in the copper "strip" seen in Fig. 1(a), which leads to a thermal resistance shown in Fig. 1(c). This joint is a necessity to facilitate removal/insertion of the sample. In other words, the difference in timescales is an indicator of the quality of the thermal path between P_3, P_4, and the cold finger. Given the placement of the heating resistor, if the heat flow through both HFSs is not equally split, then the total power Q supplied by the strain gauge can be written as

$$Q = \frac{|V_{P_3}|}{S_{P_3}} + \frac{|V_{P_4}|}{S_{P_4}} = (|V_{P_3}| + |V_{P_4}|/f)/S_{P_3}, \quad (13)$$

$$S_{P_3} = (|V_{P_3}| + |V_{P_4}|/f)/Q, \quad (14)$$

$$S_{P_4} = (|V_{P_3}|f + |V_{P_4}|)/Q, \quad (15)$$

where f is the ratio S_{P_4}/S_{P_3} determined from calibration mode (a). Therefore, by applying Eqs. (14) and (15) to the data obtained from calibration mode (b) alongside the ratio, f, determined from calibration mode (a), the sensitivities of HFSs P_3 and P_4 can be determined as a function of temperature, as shown in Fig. 2(d).

B. Example measurements

Once calibrated, several tests of the insert were run to assess the available heating power as a function of temperature, and these are summarized in Fig. 3. The sample initially considered was a
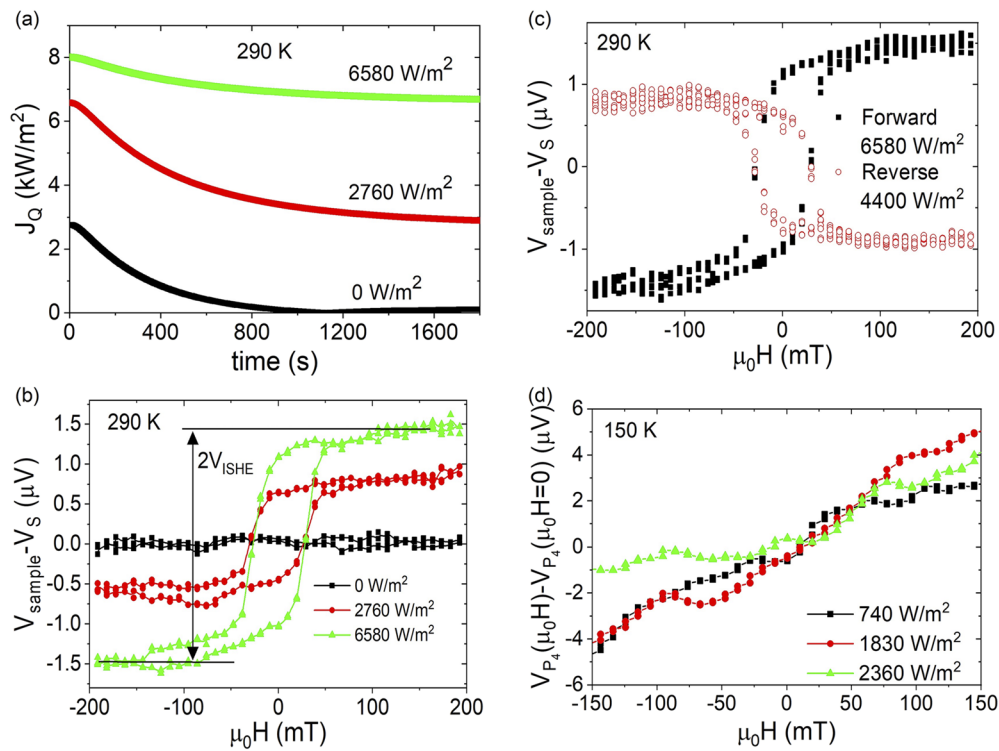
FIG. 3. Example SSE data as a function of applied magnetic field and heating option. (a) The transient heat flux through the sample relaxed by 30 min for each applied heat flux at 290 K. (Measurements were obtained with decreasing J_Q.) (b) $V_{sample} − V_S$ as a function of applied magnetic field for different measured heat fluxes at 290 K. The arrows show the calculation of V_{ISHE}, which is shown in Fig. 4. (c) Observed reversal in sign of $V_{sample} − V_S$ when the temperature gradient direction is reversed at 290 K. (d) The variation of the HFS P_4 voltage with magnetic field. A 10 point average was taken to reduce the scatter in the data.

320 nm/5 nm $SiO_2/Fe_3O_4/Pt$ grown using pulsed laser deposition and described elsewhere.[7,11] The area of the sample and contact separation was $A = 26$ mm^2 and $L_y = 3.5$ mm, respectively. The heat flux across the sample was applied by heating and cooling the activating Peltiers P_1 and P_2 using the thermal circuit described in Fig. 1(c). Figure 3(a) shows the transient measurement as heat was applied to the sample (recorded by P_3). We can observe that the heat flux stabilized by 1800 s, which was the transient settle time used for all measurements. This was used as an upper limit of the settling time, and depending on the heating direction, a lower value can be used [as shown in Figs. 2(a) and 2(c)]. We also note that the value of 1800 s is much lower than other low temperature SSE measurements where Peltiers are used to heat the sample.[20] Figure 3(b) shows the Seebeck subtracted sample voltage ($V_{sample} − V_S$) measured as a function of applied magnetic field ($\mu_0 H$) and different heat fluxes. The reversal in sign with field is a signature of the ISHE as the magnetization direction reverses and confirms that a magnetothermal signal is indeed being measured. Figure 3(c) shows the reversal in sign of the data when heating from the other direction [i.e., reversal of the heat path shown in Fig. 1(c)]. Note that due to the differing thermal paths between the HFSs and the cold finger [indicated in Fig. 1(c)], the available heating power is lower when heating from the P_2 side. Once normalized according to Eq. (3), both datasets indicate $S_{J_Q} = 47.5 \pm 2.4$ nV m W^{-1}. Finally, Fig. 3(d) shows the variation

in the HFS signal as a function of applied magnetic field for different heat flux, where the value at $\mu_0 H = 0$ has been subtracted from each dataset to make it easier to observe the field variation. This is shown for 150 K, as the increase in Johnson noise made it difficult to observe at higher temperatures. Note that for the J_Q range studied here, there is only a 0.02%–0.04% variation in V_{P_4} when a field of 150 mT is applied.

Figure 4 shows a summary of example measurements of an 80 nm/5 nm $SiO_2/Fe_3O_4/Pt$ thin film as a function of temperature. The area of the sample and contact separation was $A = 27$ mm^2 and $L_y = 4.4$ mm, respectively. We limited the measurements to a base temperature of 50 K due to concerns of the stability of the HFSs to thermal cycling as well as due to the increased heating power required at lower temperatures to generate a measurable V_{ISHE} [as indicated by the range of heating powers shown in Fig. 4(a)], which would affect the cooling power of the cryostat. In Fig. 4(a), we show the variation of V_{ISHE} with measured J_Q, and the slope of this is used to find the heat flux SSE coefficient S_{J_Q}. Figure 4(b) shows the variation of S_{J_Q} with temperature, and the general decrease in S_{J_Q} with temperature is consistent with previous reports of $S_{\nabla T}$ for Fe_3O_4[21] and YIG.[22–24] This is attributed to the decrease in magnon population at lower temperatures. These thin films had a metal–insulator Verwey transition[25] temperature of 117 K,[7] and we can see that while the SSE does not show an appreciable transition at this temperature,
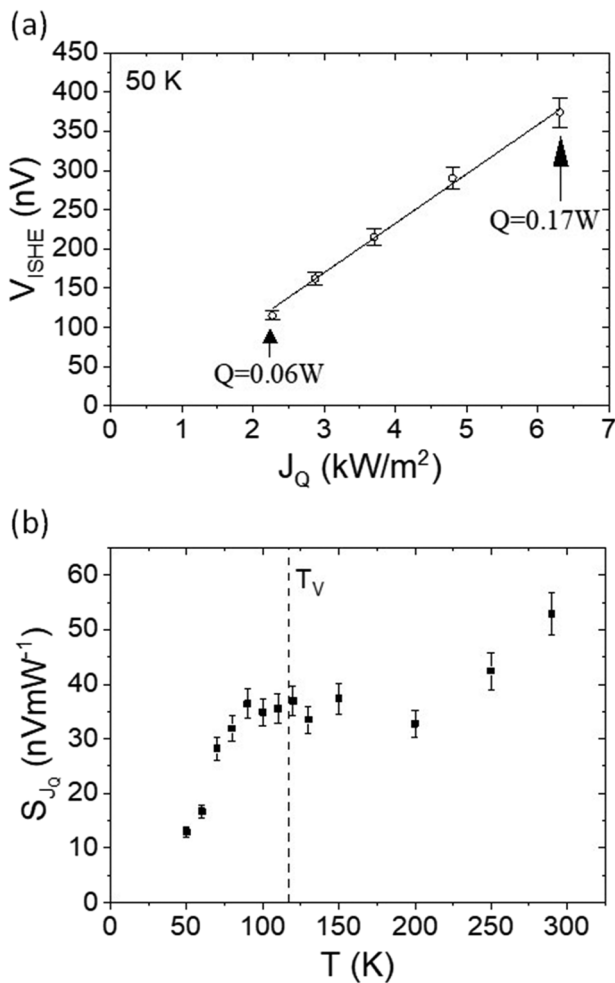
FIG. 4. Example SSE data for Fe_3O_4:Pt thin film. (a) V_{ISHE} [shown by the arrows in Fig. 3(b)] as a function of heat flux, J_Q, at 50 K, where the gradient was used to determine the normalized coefficient, S_{J_Q}, defined in the text. Also indicated is the range of heating powers supplied. (b) Normalized coefficient as a function of temperature, where the position of the Verwey transition, T_V, is indicated.

a plateau in the decrease of S_{J_Q} was observed. It is interesting to note that the peak observed between 50 K and 100 K mirrors the variation of the thermal conductivity κ previously seen for Fe_3O_4 thin films of comparable thickness,[26] and this might explain the lack of this feature in the $S_{\nabla T}$ response from Eq. (2), which was reported by Ramos *et al.*[21]

For context, it should be noted that the spin Seebeck coefficient, $S_{\nabla T}$ [Eq. (2)], reported in the literature can vary due to chosen substrate, Pt and Fe_3O_4, thicknesses. For example, Caruana *et al.*[7] compared two similar bilayers (80 nm Fe_3O_4/5 nm Pt) deposited on glass[7] where $\frac{S_{\nabla T}}{L_z} = 35.7 \ \mu V \ K^{-1} \ m^{-1}$ and (50 nm Fe_3O_4/5 nm Pt) deposited on $SrTiO_3$[27] where $\frac{S_{\nabla T}}{L_z} = 150 \ \mu V \ K^{-1} \ m^{-1}$. When the thermal conductivity of the substrate was accounted for, they reported that $\frac{S_{\nabla T}}{L_z} = 0.6 \ V \ K^{-1} \ m^{-1}$

and 0.58 $V \ K^{-1} \ m^{-1}$ for the Fe_3O_4/Pt on glass and $SrTiO_3$, respectively. As the room temperature value of S_{J_Q} measured here was 47.5 nV m W^{-1} for the (80 nm Fe_3O_4: 5 nm Pt) film deposited on glass, multiplying by the thermal conductivity (4.5 W/m/K[7]) gives $S_{\nabla T} = 0.21 \ \mu V \ K^{-1}$, and for comparison, dividing by the Fe_3O_4 thickness (80 nm) results in $\frac{S_{\nabla T}}{L_z} = 2.6 \ V \ K^{-1} \ m^{-1}$. This is significantly higher than measurements reported elsewhere as thermal resistances do not dominate this measurement, as was highlighted by Sola *et al.* in earlier demonstrations of the heat flux method[10] and in a recent round robin comparison of YIG:Pt.[9]

In conclusion, we have developed an apparatus for simultaneously measuring the spin Seebeck response and heat flux passing through magnetic thin films from 300 K down to 50 K. The measurement involves accurately calibrating the performance of heat flux sensors and then measuring the inverse spin Hall signal from the sample as a function of applied heat flux and magnetic field at different sample temperatures in a cryostat. The simplicity of the measurement means that the spin Seebeck response can be accurately determined in thin films, whereby multiplying out by the thermal conductivity of the magnetic film, a coefficient normalized by the temperature gradient can be obtained. We hope that this measurement apparatus can contribute to progressing the state of the art in understanding the microscopic mechanism of the SSE in various material systems as well as developing spin Seebeck based energy harvesting devices.

ACKNOWLEDGMENTS

DATA AVAILABILITY

All supporting data will be made available via the Loughborough data repository via https://doi.org/10.17028/rd.lboro.11931669.

REFERENCES

[1]K. Uchida, S. Takahashi, K. Harii, J. Ieda, W. Koshibae, K. Ando, S. Maekawa, and E. Saitoh, Nature **455**, 778 (2008).

[2]G. E. Bauer, E. Saitoh, and B. J. Van Wees, Nat. Mater. **11**, 391 (2012).

[3]K. Uchida, M. Ishida, T. Kikkawa, A. Kirihara, T. Murakami, and E. Saitoh, J. Phys.: Condens. Matter **26**, 343202 (2014).

[4]C. M. Jaworski, J. Yang, S. Mack, D. D. Awschalom, J. P. Heremans, and R. C. Myers, Nat. Mater. **9**, 898 (2010).

[5]S. M. Wu, W. Zhang, K. C. Amit, P. Borisov, J. E. Pearson, J. S. Jiang, D. Lederman, A. Hoffmann, and A. Bhattacharya, Phys. Rev. Lett. **116**, 097204 (2016).

[6]S. M. Wu, J. E. Pearson, and A. Bhattacharya, Phys. Rev. Lett. **114**, 186602 (2015).

[7]A. J. Caruana, M. D. Cropper, J. Zipfel, Z. Zhou, G. D. West, and K. Morrison, Phys. Status Solidi RRL **10**, 613 (2016).

[8]G. Venkat, T. Rose, C. D. W. Cox, G. B. G. Stenning, A. J. Caruana, and K. Morrison, Europhys. Lett. **126**, 37001 (2019).

[9]A. Sola, V. Basso, M. Kuepferling, M. Pasquale, D. C. ne Meier, G. Reiss, T. Kuschel, T. Kikkawa, K. Uchida, E. Saitoh *et al.*, IEEE Trans. Instrum. Meas. **68**, 1765 (2018).

[10]A. Sola, P. Bougiatioti, M. Kuepferling, D. Meier, G. Reiss, M. Pasquale, T. Kuschel, and V. Basso, Sci. Rep. **7**, 46752 (2017).

[11]G. Venkat, C. D. W. Cox, D. Voneshen, A. J. Caruana, A. Piovano, M. D. Cropper, and K. Morrison, Phys. Rev. Mater. **4**, 075402 (2020).

[12] A. Rastogi, Z. Li, A. V. Singh, S. Regmi, T. Peters, P. Bougiatioti, D. Carsten né Meier, J. B. Mohammadi, B. Khodadadi, T. Mewes, R. Mishra, J. Gazquez, A. Y. Borisevich, Z. Galazka, R. Uecker, G. Reiss, T. Kuschel, and A. Gupta, Phys. Rev. Appl. **14**, 014014 (2020).

[13] C. D. W. Cox, A. J. Caruana, M. D. Cropper, D. M. Tatnell, C. J. Kinane, T. R. Charlton, and K. Morrison, Proc. SPIE **10357**, 1035731 (2017).

[14] J. Hirschner, M. Maryško, J. Hejtmánek, R. Uhrecký, M. Soroka, J. Buršík, A. Anadón, M. H. Aguirre, and K. Knížek, Phys. Rev. B **96**, 064428 (2017).

[15] K. Mallick, A. A. Wagh, A. Ionescu, C. H. W. Barnes, and P. S. A. Kumar, Phys. Rev. B **100**, 224403 (2019).

[16] K. Mallick, A. A. Wagh, and P. S. A. Kumar, J. Magn. Magn. Mater. **492**, 165644 (2019).

[17] F. K. Dejene, J. Flipse, and B. J. Van Wees, Phys. Rev. B **86**, 024436 (2012).

[18] J. Shan, L. J. Cornelissen, J. Liu, J. Ben Youssef, L. Liang, and B. J. van Wees, Phys. Rev. B **96**, 184427 (2017).

[19] E. Jia Guo, J. Cramer, A. Kehlberger, C. A. Ferguson, D. A. MacLaren, G. Jakob, and M. Kläui, Phys. Rev. X **6**, 031012 (2016).

[20] V. Kalappattil, R. Geng, R. Das, M. Pham, H. Luong, T. Nguyen, A. Popescu, L. M. Woods, M. Kläui, H. Srikanth, and M. H. Phan, Mater. Horiz. **7**, 1413 (2020).

[21] R. Ramos, T. Kikkawa, A. Anadón, I. Lucas, K. Uchida, P. A. Algarabel, L. Morellón, M. H. Aguirre, E. Saitoh, and M. R. Ibarra, AIP Adv. **7**(5), 055915 (2017).

[22] H. Jin, S. R. Boona, Z. Yang, R. C. Myers, and J. P. Heremans, Phys. Rev. B **92**(5), 054436 (2015).

[23] T. Kikkawa, K. Uchida, S. Damon, Z. Qiu, Y. Shiomi, and E. Saitoh, Phys. Rev. B **92**, 064413 (2015).

[24] R. Iguchi, K. Uchida, S. Daimon, and E. Saitoh, Phys. Rev. B **95**, 174401 (2017).

[25] E. J. W. Verwey, Nature **144**(3642), 327 (1939).

[26] N.-W. Park, W.-Y. Lee, J.-A. Kim, K. Song, H. Lim, W.-D. Kim, S.-G. Yoon, and S.-K. Lee, Nanoscale Res. Lett. **9**, 96 (2014).

[27] R. Ramos, T. Kikkawa, K. Uchida, H. Adachi, I. Lucas, M. H. Aguirre, P. Algarabel, L. Morellón, S. Maekawa, E. Saitoh, and M. R. Ibarra, Appl. Phys. Lett. **102**(7), 072413 (2013).